Microstructure and Rheology of Thermoreversible Nanoparticle Gels

S. Ramakrishnan† and C. F. Zukoski*,‡

Department of Chemical and Biomedical Engineering, Florida A&M−Florida State University, Tallahassee, Florida 32310, and Department of Chemical and Biomolecular Engineering, University of Illinois at Urbana−Champaign, Urbana, Illinois 61801

Received January 17, 2006. In Final Form: June 15, 2006

Naïve mode coupling theory is applied to particles interacting with short-range Yukawa attractions. Model results for the location of the gel line and the modulus of the resulting gels are reduced to algebraic equations capturing the effects of the range and strength of attraction. This model is then applied to thermo reversible gels composed of octadecyl silica particles suspended in decalin. The application of the model to the experimental system requires linking the experimental variable controlling strength of attraction, temperature, to the model strength of attraction. With this link, the model predicts temperature and volume fraction dependencies of gelation and modulus with five parameters: particle size, particle volume fraction, overlap volume of surface hairs, and theta temperature. In comparing model predictions with experimental results, we first observe that in these thermal gels there is no evidence of clustering as has been reported in depletion gels. One consequence of this observation is that there are no additional adjustable parameters required to make quantitative comparisons between experimental results and model predictions. Our results indicate that the naïve mode coupling approach taken here in conjunction with a model linking temperature to strength of attraction provides a robust approach for making quantitative predictions of gel mechanical properties. Extension of model predictions to additional experimental systems requires linking experimental variables to the Yukawa strength and range of attraction.

I. Introduction

Over a narrow range of volume fractions or parameters that control strength of attraction such as temperature, pH, or ionic strength,[1,2] colloidal suspensions often gel. The gelled state is characterized by long relaxation times, apparent yield stresses, and elastic moduli that are weakly dependent on strain frequency. Gels are observed when the solids content ranges from a few volume percent to those characteristic of glasses (i.e., approaching random close packing). The volume fraction where a gel is first observed decreases as the strength of interparticle attraction increases. The material properties of gels, important in soil mechanics, mineral processing, and consumer products, have seen enormous interest.[3−14] The goal of much of this work has been to explain the volume fraction, ϕ, dependence of yield stress, viscosity, and/or elastic moduli and absolute magnitude of mechanical properties based on an understanding of particle interaction energies. Often the models are based on an assumed gel microstructure, and recent work has often assumed that this microstructure is fractal in nature. As a result, mechanical properties are expected to have a power law dependence on volume fraction with the power law exponent being a function of the gel's fractal dimension.

Alternative models related to the percolation transition have been used to describe the mechanical properties of gels.[7,15−16] A threshold volume fraction ϕ_g representing the minimum volume fraction necessary for a sample to form an infinite cluster is used in percolation theory to describe the relative distance from the gel point. Percolation models predict the elastic modulus (G') to scale as $G' \sim (\phi - \phi_g)^s$ or $(\phi/\phi_g - 1)^p$ where ϕ is the colloid volume fraction and s and p are critical exponents. Previous work showed that these scalings were observed in different systems near the gel point. Although these studies captured the volume fraction dependence of the modulus above the gel point, limited progress was made in predicting the absolute magnitude of the modulus or in predicting ϕ_g.

Recognition of the dynamic nature of gel transition has recently emerged with the successful application of mode coupling theories to hard sphere glasses and gels.[13,14,17−19] These models base their predictions of the gel point on knowledge of density fluctuations as captured in the equilibrium structure factor and predict a gel point based on particles being localized. In naïve mode coupling theory, NMCT, the suspension is treated within the framework of an Einstein solid where localized particles have a Gaussian positional dependence with a characteristic localization length, r_{loc}. Below the gel point, this localization length is infinite indicating that the particles undergo long-range self-diffusion. Localization is predicted to be the result of nearest neighbor crowding and interparticle attractions where particles are localized due to the formation of "bonds". In its original

* Corresponding author. E-mail: czukoski@uiuc.edu.
† Florida A&M−Florida State University.
‡ University of Illinois at Urbana−Champaign.

(1) Russel, W. B.; Saville, D. A.; Schowalter, W. R. *Colloidal Dispersions*; Cambridge University Press: New York, 1989.
(2) Lewis, J. A. *J. Am. Ceram. Soc.* **2000**, *83*, 2341.
(3) Buscall, R.; Mills, P. D. A.; Goodwin, J. W.; Lawson, D. W. *J. Chem. Soc., Faraday Trans.* **1988**, *84*, 4249.
(4) Chen, D. H.; Doi, M. *J. Colloid Interface Sci.* **1999**, *212*, 286.
(5) Derooij, R.; Vandenende, D.; Duits, M. H. G.; Mellema, J. *Phys. Rev. E* **1994**, *49*, 3038.
(6) Goodwin, J. W.; Hughes, R. W.; Partridge, S. J.; Zukoski, C. F. *J. Chem. Phys.* **1986**, *85*, 559.
(7) Grant, M. C.; Russel, W. B. *Phys. Rev. E* **1993**, *47*, 2606.
(8) Potanin, A. A.; Derooij, R.; Vandenende, D.; Mellema, J. *J. Chem. Phys.* **1995**, *102*, 5845.
(9) Shih, W. H.; Shih, W. Y.; Kim, S. I.; Liu, J.; Aksay, I. A. *Phys. Rev. A* **1990**, *42*, 4772.
(10) Trappe, V.; Weitz, D. A. *Phys. Rev. Lett.* **2000**, *85*, 449.
(11) Varadan, P.; Solomon, M. J. *Langmuir* **2001**, *17*, 2918.
(12) Yanez, J. A.; Laarz, E.; Bergstrom, L. *J. Colloid Interface Sci.* **1999**, *209*, 162.
(13) Bergenholtz, J.; Poon, W. C. K.; Fuchs, M. *Langmuir* **2003**, *19*, 4493.
(14) Bergenholtz, J.; Fuchs, M. *Phys. Rev. E* **1999**, *59*, 5706.
(15) Stauffer, D.; Coniglio, A.; Adam, A. *Adv. Polym. Sci.* **1982**, *44*, 103.
(16) Stauffer, D. *Introduction to Percolation Theory*; Taylor and Francis: London, 1985.
(17) Chen, Y. L.; Schweizer, K. S. *J. Chem. Phys.* **2004**, *120*, 7212.
(18) Bergenholtz, J.; Fuchs, M. *J. Phys.: Condens. Matter* **1999**, *11*, 10171.
(19) Schweizer, K. S.; Saltzman, E. J. *J. Chem. Phys.* **2003**, *119*, 1181.

10.1021/la060168j CCC: $33.50
Published on Web 08/03/2006

form, the MCT approach predicts that particles are at equilibrium locally, or inside their cages, but longer wavelength density fluctuations do not decay. Locating the gel point then becomes an exercise in determining when r_{loc}^{-1} becomes finite for the first time as strength of attraction or volume fraction are increased. Detailed calculations[17,20] show that, for a fixed strength of attraction, as volume fraction is increased above that characterizing the gel point r_{loc} shrinks. As the characteristic suspension elasticity is $\phi kT/r_{loc}^2$, strong volume fraction dependencies of $G'(\phi)$ are associated with the volume fraction dependence of r_{loc}. Of particular interest here is that these models predict mechanical properties of the gel based on equilibrium structure factors and do not assume that the gel has a fractal microstructure.

MCT predictions have been extensively tested for depletion systems consisting of hard spheres in the presence of nonadsorbing polymer.[20−22] Predictions of the gel point and mechanical properties depend on the equilibrium microstructure and thus on the suspension structure factor, $S(q)$. For depletion systems, Fuchs and Schweizer [23,24] have developed an integral equation description of $S(q)$ and these descriptions have been extensively tested and verified such that, with no adjustable parameters, subtle details of $S(q)$ can be predicted in the equilibrium state. MCT predictions of the dependencies of the location of gelation and mechanical properties of the gel on polymer radius of gyration, R_g, and polymer concentration, c_p, and particle volume fraction have all been verified for volume fractions greater than ∼0.3. However, elastic moduli are found to be a factor of ∼100 smaller than those predicted. This factor, which is essentially independent of ϕ, R_g, or c_p, has been attributed the formation of dense clusters.[21,22] The clusters are experimentally observed in scattering experiments at low scattering wave vectors, q, with cluster sizes, ξ, found to be independent of ϕ, R_g, and c_p and to consist of dense clusters 4−6 particles in diameter. Using a simple mixing rule to postulate $G' = (D/\xi)^3 G'_{MCT}$, where D is the particle diameter, G' is the measured modulus, and G'_{MCT} is the modulus predicted by MCT, and ξ is held constant independent of system variables, excellent quantitative agreement is found between predicted and measured moduli. This ad hoc rescaling is supported by the experimental evidence that the sizes of the dense clusters are independent of changes in system variables.

That the success of NMCT models is accomplished without reference to fractal dimension of particle aggregates is particularly noteworthy. NMCT predicts power law dependencies of modulus on volume fraction in both dilute and dense particulate gels as a result of the volume fraction dependence of r_{loc} and not as a result of the assumption of fractal microstructure. However, the success of the model to make quantitative predictions of gel mechanical properties is limited by a poor understanding of the origin of the dense clusters and what controls their size.

The success of the NMCT approaches to predicting the location of gel boundary and mechanical properties of depletion gels can be attributed to working with a model system where a great deal is known about equilibrium properties. Unfortunately, in dealing with less well understood attractions, extending NMCT requires linking experimental variables to parameters used to predict $S(q)$. In principle this can be accomplished by postulating a pair potential and calculating the structure factor and then validating that the interaction parameters capture the microstructure or equilibrium thermodynamics of the system of interest. One approach has been to use the adhesive hard sphere, AHS, potential for which simple analytical expressions for $S(q)$ are known.[25] This model has the advantage of describing interactions in terms of two parameters: particle diameter and the adhesiveness parameter. Unfortunately, in our hands, we find that use of the AHS $S(q)$ does not result in physically reasonable solutions for G' (i.e., modulus is predicted to decrease with increasing strength of attraction). This may be due to the unphysical nature of the pair potential.[26]

In an attempt to extend NMCT predictions to a wider range of experimental systems, here we propose applying the hard core Yukawa potential where analytical expressions are available for S(q). The Yukawa potential describes pair interactions in terms of three parameters: particle diameter, the strength of the attraction at contact, ϵ/kT, and the characteristic length of the attraction, κ^{-1}. Given recent studies demonstrating that both the strength and range of the potential are important in describing the equilibrium and nonequilibrium behavior of attractive colloidal systems[22,27] developing a model that captures these dependencies provides a more physically sound representation when developing a general approach to describing gelation in colloidal systems.

Unfortunately, there are few systems where we know how experimentally determinable parameters alter strength and range of colloidal pair potentials. This limitation means that we cannot apply the Yukawa based MCT models to an experimental system without first calibrating how ϵ and κ^{-1} change with experimental variables. In this paper, we provide an approach to resolving this problem. We work with thermally reversible gels based on octadecyl silica particles suspended in decalin.[28] This system has been extensively studied, and ϵ is thought to have the form $\epsilon/kT = A(T_\theta/T - 1)$,[29] where A and T_θ are particle size and solvent dependent constants and T is the absolute temperature of the suspension. Below we develop a method for determining A, T_θ, and κ^{-1} from knowledge of the temperature dependence of the gel line and experimental measurements of elastic moduli.

Of particular interest is that, although we extend application of the NMCT approach from depletion systems with four experimental controlling parameters ($2R_g/D$, c_p, ξ, and ϕ) required to describe $S(q)$ and G' to a system with four parameters (κD, A, T_θ, and ϕ), the thermal gels show no evidence of dense cluster formation upon gelation. As a result, there is no need to use an ad hoc rescaling to make absolute predictions of modulus.

We would like to mention here that the system used in this work is different than other systems in the literature where clustering is seen. Verduin and Dhont[30] studied octadecyl silica in benzene where a liquid−liquid-phase transition is the predominant phase transition and complicates the gelation transition. Solomon and Varadan[31] worked on octadecyl silica in hexadecane. Their work dealt with very low volume fractions ($0.01 < \phi < 0.075$) where some fractal clustering is seen. However, the cluster radius rapidly decreases to $2a$ (where a is the particle radius) at a volume fraction of 0.1. Hence, one would expect to see negligible clustering in these systems at higher volume fractions (>0.25). As one increases volume fraction and moves into the dense suspension regime, fractal arguments used to describe the structure of colloidal gels fail as a fractal floc will

(20) Shah, S. A.; Chen, Y. L.; Schweizer, K. S.; Zukoski, C. F. *J. Chem. Phys.* **2003**, *119*, 8747.
(21) Ramakrishnan, S.; Gopalakrishnan, V.; Zukoski, C. F. *Langmuir* **2005**, *21*, 9917.
(22) Ramakrishnan, S.; Chen, Y. L.; Schweizer, K. S.; Zukoski, C. F. *Phys. Rev. E* **2004**, *70*, 040401 (R).
(23) Fuchs, M.; Schweizer, K. S. *Phys. Rev. E* **2001**, *64*, 021514.
(24) Fuchs, M.; Schweizer, K. S. *J. Phys.: Condens. Matter* **2002**, *14*, R239.
(25) Regnaut, C.; Ravey, J. C. *J. Chem. Phys.* **1989**, *91*, 1211.
(26) Stell, G. *J. Stat. Phys.* **1991**, *63*, 1203.
(27) Shah, S. A.; Chen, Y. L.; Schweizer, K. S.; Zukoski, C. F. *J. Chem. Phys.* **2003**, *118*, 3350.
(28) Rueb, C. J.; Zukoski, C. F. *J. Rheol.* **1997**, *41*, 197.
(29) Jansen, J. W.; Dekruif, C. G.; Vrij, A. *J. Colloid Interface Sci.* **1986**, *114*, 471.
(30) Verduin, H.; deGans, B. J.; Dhont, J. K. G. *Langmuir* **1996**, *12*, 2947.
(31) Solomon, M. J.; Varadan, P. *Phys. Rev. E* **2001**, *63*, 051402(1−10).

have a diameter only a few times that of the primary particle. The volume fraction range studied in this work ($0.25 < \phi < 0.45$) is different from that of Solomon and Varadan. It is possible that at low volume fractions the octadecyl silica particles in decalin might also form clusters. Rueb and Zukoski[28] reported on the scattering of gels of octadecyl silica particles suspended in tetradecane and found evidence of clustering by neutron scattering measurements. The solvent used in this work is decalin. All of the systems used above are different than in the work reported here. We conclusively do not see any clustering in our octadecyl silica system in decalin, from both X-ray and neutron scattering measurements.[21] Thus, the octadecyl silica/decalin system serves as an ideal system to test the validity of predictions of the naïve mode coupling theory since the ad hoc rescaling is not required.

Below in section II, we describe the experimental system used. Section III reviews the major predictions of naïve mode coupling theory (MCT). Progress can only be made with predictions of $S(q)$. For this purpose, we use the predictions of Cummings and Smith[32] with a modification to account for the inadequacies of the MSA closure as suggested by Bergenholtz.[33] We briefly describe the effects of changes in system parameters on predicted mechanical properties in section IV before turning to application of this model to the thermoreversible gels in section V. Conclusions are drawn in section VI.

II. Experimental Section

Silica particles ($D = 90 \pm 6$ nm) were prepared by the base-catalyzed hydrolysis and condensation of tetra ethyl orthosilicate according to the method of Stober, Fink, and Bohn[34] and a seeded growth technique of Bogush and Zukoski[35] to increase the particle diameter. The particles were then rendered hydrophobic via the method of van Helden, Jansen, and Vrij[36] and characterized with electron microscopy, ultra-small-angle X-ray scattering, and dynamic light scattering. The synthesized particles had a gravimetrically determined density of $\rho_c = 1.9 \pm 0.04$ g/mL. Suspensions were prepared by dispersing a known mass of dried silica powder in 50:50 mixture of cis and trans-decalin followed by stirring to better disperse the powder. The volume fractions were also determined by dry weight using $\phi = c/\rho_c$, where c is the mass concentration (g/mL) of the silica in suspension.

The phase diagram of thermal gels was measured rheologically. The gel temperature at a particular volume fraction was taken to be the temperature at which the elastic modulus measured at 1 Hz just falls below the loss modulus. Rheological measurements for the thermal gels were performed using a Bohlin CVO constant stress rheometer with a temperature control of ±0.2 °C fitted with a cup and bob geometry with a 14 mm bob diameter and fixed outer cup diameter of 15.4 mm yielding a tool gap of 0.7 mm. A known volume (3 mL) of the sample was loaded into the rheometer at room temperature where the samples are easily flowing fluids and cooled to the desired temperature of measurement and allowed to equilibrate. Measurements of the elastic modulus were then made (with and without pre-shear) at a fixed oscillatory frequency of 1 Hz until the system reaches a state of mechanical equilibrium as shown by the plateau of the elastic modulus with time.

Ultra-small-angle X-ray scattering (USAXS) experiments were conducted at the UNICAT facility on the 33-ID line, Advanced Photon Source (APS) facility at Argonne National Laboratory. Similar to the rheological measurements, scattering measurements were made at a fixed temperature and varying ϕ and then repeated for different temperatures. Details of the instrumental setup are given elsewhere.[37] The instrument utilizes a Bonse-Hart camera using Si(111) optics with additional side-reflection stages enabling effective pinhole collimation where desmeared data are obtained. The beam is 0.4 mm vertical by 1.5 mm horizontal through which 2×10^{13} photons are incident at 10 keV with a wavelength $\lambda = 1.54$ Å. The instrument has a q range of 2×10^{-4}–2×10^{-1} Å^{-1} with a resolution of $\Delta q = 2 \times 10^{-4}$ Å^{-1}. The scattered beam is analyzed by rotating Si(111) channel cut crystal and measured by a photodiode detector. The narrow wavelength resolution ($\Delta\lambda/\lambda = 1.5 \times 10^{-4}$) ensures wavelength smearing effects are insignificant. All samples were loaded in custom-made aluminum cell holders with a 1 mm beam path length, enclosed between two Kapton polyimide film windows.

III. Naïve Mode Coupling Theory Applied to Yukawa Attractions

A recently developed extension of mode coupling theory, naïve mode coupling theory, NMCT, provides a facile method to approximate the predictions of the full mode coupling approach.[17,19] Within the context of mode coupling theories, at the gel point, the particles are localized and cannot diffuse over distances large compared to a particle diameter. Starting from the equations of motion, the NMCT approach develops an expression for the localization length or maximum root-mean-square diffusive displacement of the particle r_{loc}^2

$$\frac{1}{r_{loc}^2} = \frac{1}{9}\int_0^\infty \frac{4\pi q^2 dq}{(2\pi)^3} q^2 \rho C^2(q) S(q) e^{-q^2 r_{loc}^2/6(1+1/S(q))} \quad (1)$$

where q is the momentum transfer vector, ρ is the particle number density, and $C(q)$ is the direct correlation function which can be calculated from $S(q)$. Given r_{loc} and the structure factors, the zero-frequency elastic modulus follows from the standard Green−Kubo formula plus the MCT factorization

$$G' = \frac{kT}{60\pi^2}\int_0^\infty dq q^4 \left(\frac{d \ln S(q)}{dq}\right)^2 e^{-q^2 r_{loc}^2/3(1/S(q))} \quad (2)$$

The characteristic elasticity ($G'D^3/kT$) is given by $\phi D^2/r_{loc}^2$, which can be thought of as an "effective spring constant" of an elastic network. As one moves deeper into the gel (by increasing ϕ or the strength of attraction), r_{loc} shrinks with the result being that G' increases. NMCT thus predicts both the location of the gel boundary and the mechanical properties of the gel within one model. The input into NMCT is the equilibrium structure factor for the suspension which can be calculated from a given interaction potential or measured experimentally. It should be noted here that the q region of interest of $S(q)$ in the calculations is of $O(1/r_{loc})$ or the high q region ($qD \sim 100$ typically). Thus, NMCT can be applied to dilute and dense colloidal gels. In addition, as opposed to long-range structures governing mechanical properties as is proposed in fractal models of dilute gels, NMCT predicts that the important length scale is r_{loc} which is typically a small fraction of a particle diameter.

To describe the attractions between the colloidal particles in this work, a Yukawa potential is used. The interaction energy $u_{Yukawa}(r)$ between two spherical particles in a Yukawa system is given by

$$\frac{u_{Yukawa}(r)}{kT} = \begin{cases} \infty & \text{for } r < D \\ -\frac{\epsilon}{kT}\frac{e^{-\kappa D(r/D-1)}}{r/D} & \text{for } D < r \end{cases} \quad (3)$$

where ϵ/kT is the strength of attraction at contact and κ^{-1} is a

(32) Cummings, P. T.; Smith, E. R. *Chem. Phys.* **1979**, *42*, 241.
(33) Bergenholtz, J. Personal communication, 2004.
(34) Stober, W.; Fink, A.; Bohn, E. *J. Colloid Interface Sci.* **1968**, *26*, 62.
(35) Bogush, G. H.; Tracy, M. A.; Zukoski, C. F. *J. Non-Cryst. Solids* **1988**, *104*, 95.
(36) Van Helden, A. K.; Jansen, J. W.; Vrij, A. *J. Colloid Interface Sci.* **1981**, *81*, 354.
(37) Ilavsky, J.; Allen, A.; Long, G.; Jemian, P. *Rev. Sci. Inst.* **2002**, *73*, 1660.

characteristic length of attraction. Given ϵ/kT, κD, and ϕ, one can calculate $S(q)$ for the Yukawa potential. In this work, $S(q)$ for the Yukawa system under different conditions is calculated using the code of Bergenholtz.[31] The code calculates $S(q)$ using the mean spherical approximation (MSA) closure and more details of the calculations can be found in ref 30.

Calculations of Tau and Reatto[38] have shown that the MSA is inadequate in the presence of attractions between particles which is strong and short ranged compared with the hard core diameter. Tau and Reatto found that when the strength parameter (ϵ/kT) is large, MSA can be improved if the strength of attraction used in the calculation (ϵ_{MSA}/kT) is considered as an effective strength of attraction. They demonstrated that MSA calculations of $S(q)$ were nearly identical with simulations when ϵ_{MSA}/kT is calculated by equating the MSA second virial coefficient (B_2) and the exact B_2 of the Yukawa system.

$$\int_1^\infty dx\, x^2\left\{\exp\left[\frac{\epsilon/kT}{x}e^{-\kappa D(x-1)}\right]-1\right\}=\frac{\kappa D+1}{(\kappa D)^2}\frac{\epsilon_{MSA}}{kT} \quad (4)$$

Calculations of ϵ/kT for different κD (11, 20, 50, and 100) reveal a simple correlation between ϵ/kT and ϵ_{MSA}/kT

$$\frac{\epsilon_{MSA}}{kT}=0.69e^{0.8\epsilon/kT} \quad (5)$$

Equation 5 is used in this work to relate the exact, ϵ, and MSA strengths of attraction, ϵ_{MSA}.

Below we use the Yukawa pair potential to determine gel boundaries and elastic moduli for a range of strengths and ranges of attraction.

The goal of this work is to understand how these parameters alter the volume fraction and temperature dependence of the thermal gel properties. We find that over a range of parameter space we are able to collapse the resulting behavior into straightforward algebraic expressions allowing facile estimation of κD and ϵ/kT from experimental data. These results are general in that the NMCT predictions can be applied to any system where the particles interact with short-range Yukawa potentials.

Applying these results to an experimental system is problematic because it is rare that the dependencies of κD and ϵ/kT on experimental parameters are known. To demonstrate the applicability of the NMCT predictions, we apply our results to the case of thermal gels.

Determination of r_{loc} is accomplished through solution of eq 1 at fixed ϵ_{MSA}/kT, κD, and ϕ. Shown in Figure 1, panels a and b, are plots of r_{loc}/D for a variety of conditions. When the volume fraction increases above the gel point, r_{loc} decreases in size indicating that the particles are more tightly bound and an increase in elastic modulus.

Gel boundaries (i.e., those conditions where on increasing ϕ or ϵ/kT, D/r_{loc} takes on its first nonzero value) are shown in Figure 2. The lines shown in Figure 2 are power law fits to the model calculations

$$\left(\frac{\epsilon_{MSA}}{kT}\right)_{gel}=B\phi^{-x} \quad (6)$$

Values of B and x are summarized in Table 1. As the range of attraction decreases (increasing κD), greater strengths of attractions are needed before the particles are localized. This effect is seen as an upward shift of the curves in Figure 2 with increasing κD. It should also be pointed out that all of the theoretical calculations done in this work are for volume fractions less than 0.42 as NMCT predicts localization in hard spheres at this ϕ. Hence, the correlations developed in this work which are based on the Yukawa potential are valid only for $\phi < 0.42$.

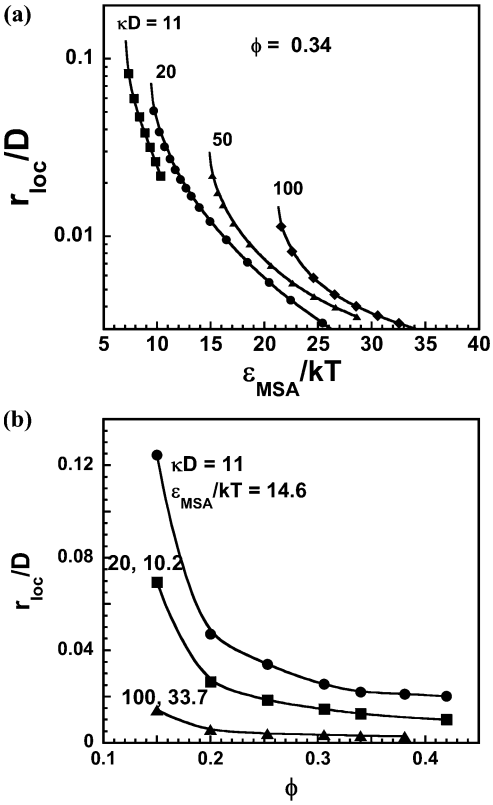

Figure 1. (a) Theoretical calculations of the localization length (r_{loc}) using NMCT and normalized by the particle diameter (D) as a function of the strength of attraction at contact (ϵ_{MSA}/kT) for particles interacting with the Yukawa potential for different values of the range of attraction (κD) at a fixed colloid volume fraction (ϕ) of 0.34. The solid symbols are theoretical calculations for different κD, and the solid lines are smooth curves drawn to guide the eye. (b) Localization length normalized by the particle diameter as calculated using NMCT for particles interacting with the Yukawa potential as a function of colloid volume fraction (ϕ). The calculations are performed at different values of κD and ϵ_{MSA}/kT which are given in the figure next to the calculations. The solid symbols are calculations at a fixed κD and ϵ_{MSA}/kT, and the solid lines are drawn to guide the eye.

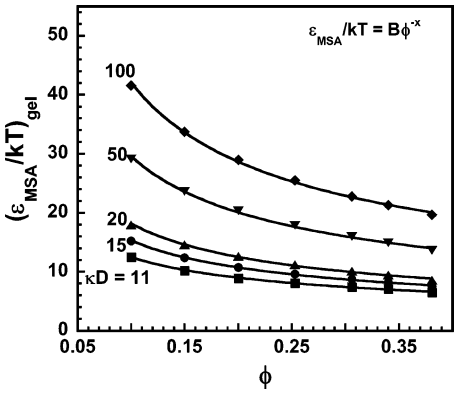

Figure 2. Calculated localization boundaries for particles interacting with the Yukawa potential using NMCT; the strength of attraction at contact ϵ_{MSA}/kT at the point of localization is plotted as a function of the colloid volume fraction ϕ at different values of the range of attraction κD. The solid symbols are theoretical calculations, and the lines are drawn to guide the eye.

(38) Tau, M.; Reatto, L. *J. Chem. Phys.* **1985**, *83*, 1921.

Table 1. Values of the Exponent (x) and Prefactor (B) Calculated from a Power Law Fit to the Yukawa Based NMCT Calculation of the Localization Boundary: $(\epsilon_{MSA}/kT)_{gel} = B\phi^{-x}$ [a]

κD	B	x	κD	B	x
11	4.2	0.47	50	8.15	0.56
15	4.68	0.52	100	11.74	0.55
20	5.26	0.54			

[a] Calculations of the gel boundary are done at a fixed value of κD which is given in the first column.

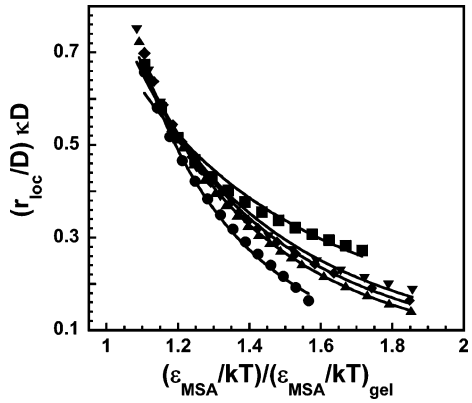

Figure 3. Calculated localization length (r_{loc}) normalized by the particle diameter (D) and scaled by the range of attraction (κD) and plotted as a function of strength of attraction at contact which is normalized by the strength of attraction at the point of localization. Calculations are performed at a fixed ϕ of 0.34 at different values of κD: 11 (●), 15 (▲), 20 (◆), 50 (▼), and 100 (■). The solid symbols are calculations, and the lines are power law fits (eq 7) to the calculated values. The power law exponents are given in Table 3.

Table 2. Values of the Exponent $\chi(\phi,\kappa D)$ in Equation 7 as Calculated from Figure 3 for Different Values of κD and ϕ

	$\chi(\phi,\kappa D)$					
κD	$\phi = 0.381$	0.34	0.306	0.253	0.2	0.15
11	3.18	3.61	3.87	4.07	3.99	3.89
15	2.75	2.98	3.11	3.18	3.16	3.06
20	2.79	2.75	2.83	2.79	2.84	2.74
50	2.39	2.42	2.57	2.51	2.56	2.46
100	1.88	1.96	1.98	1.93	1.82	1.87

Once the phase boundary has been determined, calculations of the localization length and elastic modulus can be performed as regions deeper in the gel are explored. The goal is to develop correlations for localization length and elastic moduli that will help in the interpretation of the experimental data. Figure 3 is a plot of the localization length (at $\phi = 0.34$) as a function of $(\epsilon_{MSA}/kT)/(\epsilon_{MSA}/kT)_{gel}$. This plot is similar to calculations of r_{loc} for depletion gels at different strengths of attraction (i.e., increasing polymer concentration) where all of the calculations for different ranges of attraction collapse onto a single curve when r_{loc} is normalized by the range of attraction R_g.[17,20] However, the calculations of r_{loc} using the Yukawa potential for different values of κD do not collapse onto a single curve as can be seen from Figure 3. The solid lines in Figure 3 are power law fits to the model calculations

$$\frac{r_{loc}}{D}\kappa D = F(\phi,\kappa D)\left(\frac{\epsilon_{MSA}/kT}{(\epsilon_{MSA}/kT)_{gel}}\right)^{-\chi(\phi,\kappa D)} \quad (7)$$

The values of $\chi(\phi,\kappa D)$ for a range of ϕ and κD are listed in Table 2. The range of curve fits for all volume fractions is similar to that of $\phi = 0.34$ in Figure 3. The lower limit of $(\epsilon_{MSA}/kT)/(\epsilon_{MSA}/kT)_{gel}$ for all calculations is ~1.05. For $\kappa D < 15$ the upper limit of $(\epsilon_{MSA}/kT)/(\epsilon_{MSA}/kT)_{gel}$ is ~1.6. When $[\kappa D/F(\phi,\kappa D)]^2$ is plotted as a function of κD, a simple scaling is obtained at different volume fractions

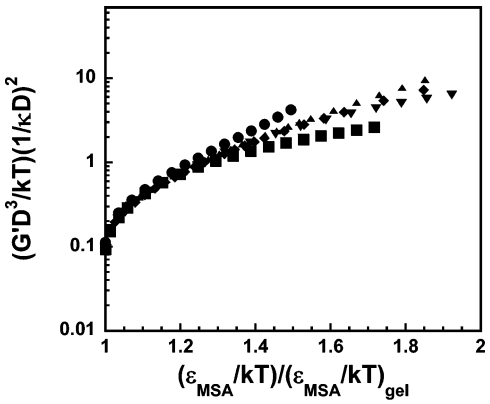

Figure 4. Yukawa-based NMCT calculations of the scaled zero frequency elastic modulus plotted as a function of the strength of attraction normalized by the strength of attraction at the localization boundary. Calculations are performed at a fixed ϕ of 0.34 at different values of κD: 11 (●), 15 (▲), 20 (◆), 50 (▼), and 100 (■).

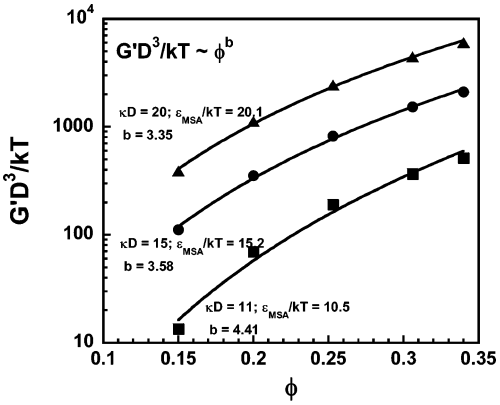

Figure 5. Yukawa-based NMCT calculations of the normalized zero frequency elastic modulus as a function of the colloid volume fraction ϕ for different values of the interaction potential parameters. The solid symbols are calculations for the given values of κD and ϵ/kT, and the lines are power law fits to ϕ. The power law exponents (b) are also given in the graph.

$$\left(\frac{\kappa D}{F(\phi,\kappa D)}\right)^2 = (3.11 - 27.31\phi + 106.37\phi^2 - 137.45\phi^3)(\kappa D)^{2.2} \quad (8)$$

Care should be taken when using eq 8, and its use should be limited to $0.15 \le \phi \le 0.381$ and $11 \le \kappa D \le 100$.

Once the localization length has been calculated for a given ϕ, ϵ_{MSA}/kT, and κD, the zero frequency elastic modulus can be evaluated using eq 2. Figure 4 is a plot of dimensionless elastic modulus ($G'D^3/kT$) at $\phi = 0.34$ as a function of $(\epsilon_{MSA}/kT)/(\epsilon_{MSA}/kT)_{gel}$ for different values of κD. To account for the increase in elasticity due to the decrease in range of attraction, the elastic moduli are scaled by $1/(\kappa D)^2$. As can be seen from Figure 4, there is reasonable collapse of the scaled elastic moduli onto a single curve for $(\epsilon_{MSA}/kT)/(\epsilon_{MSA}/kT)_{gel} < 1.5$ for all κD studied here. For typical conditions, varying the strength of attraction through this range results in changes of r_{loc}/D and G' by factors of 4 and 30 respectively from their values at the gel point.

Figure 5 is a plot of dimensionless elastic modulus at three different values of κD as a function of ϕ at fixed strengths of attraction. The solid lines are power law fits to the model

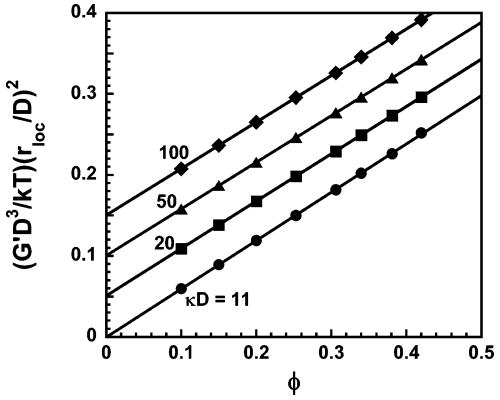

Figure 6. Yukawa-based NMCT calculations of the scaled zero frequency elastic modulus plotted as a function of the colloid volume fraction ϕ. Calculations are performed at different values of ϵ/kT at a fixed κD: $\kappa D = 11$ (●), 20 (●), 50 (▲), and 100 (◆). The calculations for $\kappa D = 20$, 50, and 100 are offset by 0.05, 0.1, and 0.15, respectively. The solid lines at each κD are linear fits to the calculations. The slope of the lines is a constant value at 0.58.

calculations. As can be seen from Figure 5, the elastic modulus varies in a power law manner with volume fraction

$$\frac{G'D^3}{kT} \approx \phi^b \tag{9}$$

Despite the variability of G' on ϕ, NMCT predicts the dependence of G' on κD and ϵ_{MSA}/kT can be captured by a single variable: the localization length (r_{loc}). Figure 6 is a plot of the elastic modulus scaled by r_{loc}^2 and plotted as a function of ϕ for different κD. Numerous calculations of G' for different values of κD and ϵ_{MSA}/kT collapse onto a single curve when plotted in this manner. The solid lines shown in the above graph are a linear fit to the data with a slope of 0.58. Thus, Figure 6 shows that the dimensionless modulus is a simple linear function of ϕ and is quantitatively given by

$$\frac{G'D^3}{kT} = 0.58\frac{\phi D^2}{r_{loc}^2} \tag{10}$$

Substituting for r_{loc}/D from eq 7 yields

$$\frac{G'D^3}{kT} = \frac{0.58\phi(\kappa D)^2}{F^2(\phi,\kappa D)}\left(\frac{(\epsilon_{MSA}/kT)_{gel}}{\epsilon_{MSA}/kT}\right)^{-2\chi(\phi,\kappa D)} \tag{11}$$

ϵ_{MSA}/kT can be related to the real strength of attraction ϵ/kT using eq 5 yielding

$$\frac{G'D^3}{kT} = \frac{0.58\phi(\kappa D)^2}{F^2(\phi,\kappa D)}\exp\left[1.6\chi(\phi,\kappa D)\left\{\left(\frac{\epsilon}{kT}\right) - \left(\frac{\epsilon}{kT}\right)_{gel}\right\}\right] \tag{12}$$

The above expression for the elastic modulus provides a simple method to extract interaction potential parameters from experimental measurements of G'. A central challenge in suspension mechanics is to relate expressions such as that shown in eq 12 to an experimental system where a priori knowledge of ϵ and κ^{-1} are not available. We introduce our experimental results below before we refine eq 12 to the thermal gel system.

IV. Results

Recently, we reported on the microstructural and mechanical properties of concentrated suspensions of depletion and thermal gels of octadecyl silica particles for different values of the strength of interaction (polymer concentration for depletion gels and temperature for thermal gels) and colloid volume fraction.[21] In that report, we systematically measured the phase boundary, microstructure, and mechanical properties (elastic modulus) of the thermal gels at different volume fractions as a function of temperature. It is our aim in the current paper to test the predictive capability of NMCT coupled with the attractive Yukawa interaction potential of the gel boundary and elastic moduli of the thermal gel system. A brief summary of the experimental findings is given below.

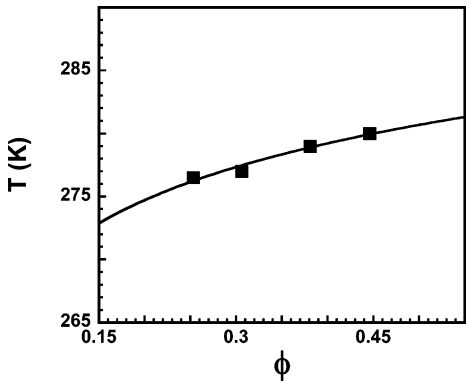

Figure 7. Gel boundary of octadecyl silica particles suspended in decalin upon reduction of temperature. The solid squares are the experimental points of the four samples studied in this work, and the line is a power law fit to the experimental data. The suspension is a fluid above the line and as one decreases the temperature and crosses the boundary, the system gels.

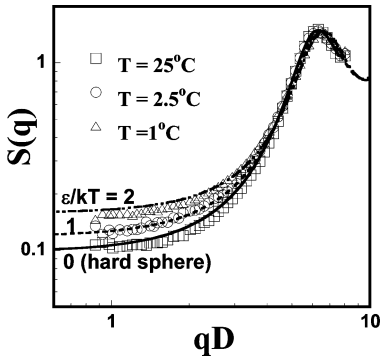

Figure 8. Structure factor ($S(q)$) of thermal gel of $\phi = 0.3$ as measured by USAXS at different temperatures: $T = 25$ °C (□), $T = 2.5$ °C (△), and $T = 1$ °C (○). The lines are calculations of $S(q)$ for the Yukawa potential at different values of ϵ/kT: 0 (hard spheres), 1, and 2. The gel point of the suspension is around 4 °C.

When suspended in decalin, the octadecyl silica particles behave as hard spheres at room temperature of 25 °C. Reduction in temperature leads to decalin becoming a poor solvent for the octadecanol hairs and hence results in a temperature induced attraction between the colloidal particles. At a particular temperature, the particles are localized and the resulting gel has a finite elastic modulus. The phase diagram of this system (determined rheologically) is shown in Figure 7 for different volume fractions. The gel line is relatively flat with $T_{gel} = 3$ °C at $\phi = 0.25$ and $T_{gel} = 7$ °C at $\phi = 0.45$. The above given gel line is very similar to the findings of Rueb and Zukoski,[28] who studied a similar thermal gel system.

Figure 8 is a plot of $S(q)$ for the thermal gels at a ϕ of 0.3 as a function of temperature. The solid line is a calculation of the hard sphere structure factor with the Percus−Yevick closure at $\phi = 0.3$. There is excellent agreement with the measured $S(q)$ at $T = 25$ °C suggesting the particles indeed behave as hard spheres at room temperature. At a volume fraction of 0.3, the suspension gels at 4 °C. As shown in Figure 8, the measured

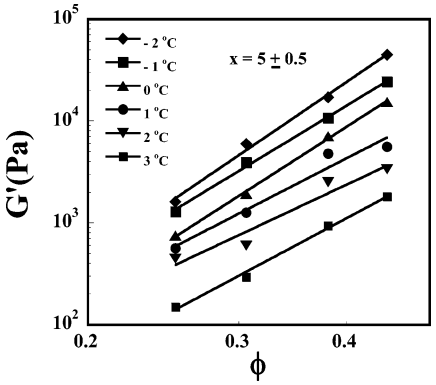

Figure 9. Measured elastic modulus as a function of volume fraction ϕ for thermal gels at different temperatures. The solid lines are power law fits to the elastic modulus $G' \sim \phi^x$ and the exponent x is a constant at 5 ± 0.5 under all of the conditions studied.

structure factor changes very little as temperature is varied from 25 to 2.5 °C. There are no upturns at low qD indicating the absence of clustering in the thermal gel systems. This is in contrast to the depletion gels where large upturns were seen at low qD indicating clusters of the size of 3−5 particle diameters. Extraction of interaction potential parameters from the measured $S(q)$ curves is difficult due to lack of changes in $S(q)$ at small values of qD and the weak dependence of $S(q)$ near the first peak on temperature. Moreover, one needs to see an appreciable change in the structure of the equilibrium liquid as one approaches the gel point so that one can curve fit the measured $S(q)$ to back out interaction potential parameters. As can be seen from Figure 8, this is not possible as the structure in the gel at 2.5 °C is hardly different from the hard sphere value at 25 °C. Shown in Figure 8 are also calculations of Yukawa $S(q)$ at a κD of 11 and at different strengths of attraction. Comparisons of $S(q)$ are made with the gelled structure (nonequilibrium) of the suspension. These equilibrium calculations which do not take into account clustering match the experimental data at low qD and at the intermediate qD, confirming that fact that clustering is absent in thermal gels. This is in contrast to the structure of depletion gels where equilibrium calculations of $S(q)$ failed to capture the structure in gel region. More details on the structure of thermal gels can be found in ref 21.

The measured elastic modulus is given as a function of volume fraction at a fixed temperature in Figure 9. The lines drawn through the data set are power law fits to G' and power law exponents of 5 ± 0.5 describe the experimental data well over a wide volume fraction range. These results are in agreement with the studies of Rueb and Zukoski,[28] who found a power law variation of elastic modulus with volume fraction for their thermal gels with a constant power law exponent of 5. It should be kept in mind that these measurements were done at 1 Hz, whereas the theory predicts the zero frequency elastic modulus. However, a frequency sweep done on these gels indicated a flat slope which means that the modulus measured at 1 Hz is a reasonable approximation to that at zero frequency.

V. Analysis and Discussion

The equation for G' from NMCT predicts an exponential dependence on the strength of attraction ϵ/kT. Following Jansen et al.[29] we connect the strength of attraction to temperature through the Flory-Krigbaum theory where Jansen et al. suggest

$$\frac{\epsilon}{kT} = A\left(\frac{T_\theta}{T} - 1\right) \text{ for } T \le T_\theta \qquad (13)$$

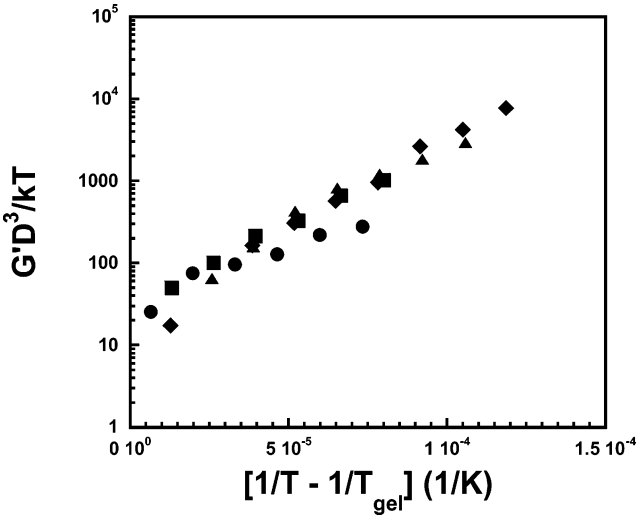

Figure 10. Experimentally measured elastic modulus (and scaled with respect to D^3/kT) as a function of $1/T - 1/T_{gel}$ where T is the temperature and T_{gel} is the gelation temperature at the given volume fraction. The symbols are the experimental measurements at different volume fractions: $\phi = 0.253$ (●), 0.306(■), 0.381(▲), and 0.446 (◆).

Table 3. Values of the Intercept, Slope, κD, and AT_θ Extracted from Figure 10 Using Equation 14[a]

ϕ	intercept	slope	κD	AT_θ	T_θ (K)	A
0.253	28.45	33 082	12.16	5630.6	327.2	17.2
0.306	30.70	45 311	11.87	7883.1	309.9	25.4
0.381	27.56	46 578	11.13	9191.4	305.1	30.1
0.446	24.00	47 092				

[a] The values of $\chi(\phi,\kappa D)$ and $F(\phi,\kappa D)$ which are used in extracting the tabulated values are calculated for the Yukawa potential using NMCT at the respective volume fractions and κD. The values of A and T_θ are determined by matching the experimental gel boundary with calculations of the NMCT gel boundary with the help of eq 13.

where A is a factor proportional to the overlapping volume of the chains and T_θ is the theta temperature of the chain solvent pair. Substituting the above expression for ϵ/kT into eq 12 yields

$$\frac{G'D^3}{kT} = \frac{0.58\phi[\kappa D]^2}{F^2(\phi,\kappa D)} \exp\left[1.6\chi(\phi,\kappa D)AT_\theta\left(\frac{1}{T} - \frac{1}{T_{gel}}\right)\right] \qquad (14)$$

Thus, to predict the elastic moduli of thermal gel systems from eq 14, one needs to determine κD, A, and T_θ. Once κD is determined for a given volume fraction, $\chi(\phi,\kappa D)$ can be looked up from Table 2 and the modulus can be predicted.

Equation 14 suggests that from a log-linear plot of G' as a function of $1/T - 1/T_{gel}$ at a fixed ϕ, κD can be determined from the intercept while the product of AT_θ can be determined from the slope. Figure 10 is a replot of the measured G' of Figure 9 as a function of $1/T - 1/T_{gel}$ at four different volume fractions. As can be seen from this figure, G' for all volume fractions scatters about a single curve when plotted in this manner. The values of the intercept, slope, κD, and AT_θ extracted from the plot are given in Table 3 for the three volume fractions for which theoretical calculations of $\chi(\phi,\kappa D)$ and $F(\phi,\kappa D)$ are known. To obtain the individual values of A and T_θ, the experimental gel boundary is matched with calculations of the NMCT gel boundary with the help of eq 13. The results are again presented in Table 3. As can be seen from Figure 10 and Table 3, the κD values obtained for the different volume fractions studied in this work lies in a narrow range. This suggests that the range of attraction of the Yukawa potential which best describes the experimental

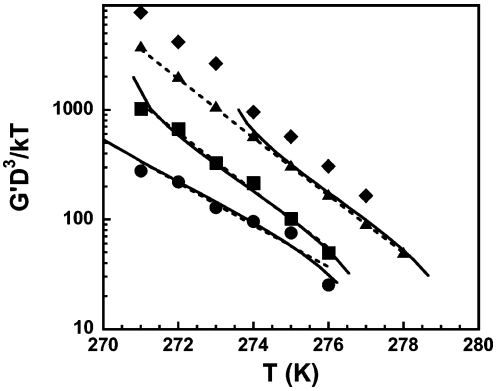

Figure 11. Scaled experimental elastic modulus as a function of temperature at different volume fractions: $\phi = 0.253$ (●), 0.306(■), 0.381(▲), and 0.446 (◆). The solid lines are calculations of NMCT with Yukawa $S(q)$ as an input at the respective volume fractions. The values of A and T_θ used in the theoretical calculations are given in Table 3. The values of κD used are 12, 12, and 11 at a ϕ of 0.253, 0.306, and 0.381, respectively. The dashed line is the correlation developed for the elastic modulus for particles interacting with the Yukawa potential (eq 14).

system at the different volume fractions is almost a constant and does not change with ϕ. The slope of Figure 10 along with the calculated value of $\chi(\phi,\kappa D)$ determines the strength of attraction at contact and hence A and T_θ. One of the assumptions in using the Yukawa potential is that the interaction potential is independent of volume fraction, whereas in the analysis, we find a weakly volume fraction dependent strength of attraction as seen by the volume fraction dependence of A and T_θ. A possible explanation for this phenomenon might be due to the role of gravity in the lower volume fraction gels ($\phi \leq 0.253$). The particle gel networks formed at these volume fractions are weaker than those at higher volume fractions and gravity might cause the network to rearrange (not to the extent of clustering of particles) thus giving rise to a lower elastic moduli than expected. This shows up as a decreased slope in Figure 10 and hence a different value of the strength of attraction at contact.

Figure 11 is a plot of the elastic modulus as a function of $1/T - 1/T_{gel}$ for the different volume fractions studied in this work. The solid line is the calculation of G' using NMCT with the Yukawa potential as an input for $S(q)$. The values of κD used are 12, 12, and 11 at a ϕ of 0.253, 0.306, and 0.381, respectively (close to the values given in Table 3). The strength of attraction in the Yukawa potential is calculated by using the values of A and T_θ in Table 3. The dashed line is the correlation (eq 14) developed for elastic modulus using NMCT and the Yukawa potential using the same values of κD, A, and T_θ. As can be seen from this graph, the developed correlation matches well with the exact calculations over the range of volume fractions and κD studied in this work.

The values of A and T_θ obtained in Table 3 are similar to the values obtained by other researchers.[29,39] Rouw and co-workers[39] determined A and T_θ to be 26.8 and 356.7 K, respectively, for octadecyl silica ($D = 63$ nm) in benzene and 53 and 314.9 K, respectively, for octadecyl silica ($D = 83$ nm) in *n*-dodecane. Jansen and co-workers[29] determined A and T_θ to be 23.2 and 345 K for octadecyl silica ($D = 70$ nm) in toluene. It should be pointed out here that the phase behavior of octadecyl silica particles is different in the various solvents and the values of A and T_θ are dependent on the solvent in which it is dispersed. Benzene and toluene lead to phase separation, whereas *n*-dodecane leads to gelation even at very low volume fractions.

(39) Rouw, P. W.; Vrij, A.; Dekruif, C. G. *Colloids Surf.* **1988**, *31*, 299.

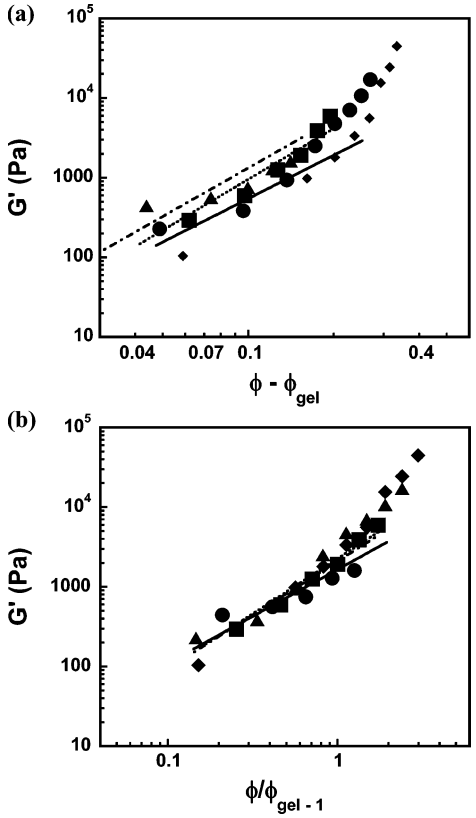

Figure 12. Elastic modulus (G') as a function of $\phi - \phi_{gel}$ (a) and $\phi/\phi_{gel} - 1$ (b), respectively. The solid symbols are the experimental measurements at different volume fractions: $\phi = 0.253$ (●), 0.306 (■), 0.381 (▲), and 0.446 (◆). The lines are power law fits to NMCT calculations: $\phi = 0.253$ (short−long dashes), 0.306 (short dashes), and 0.381 (solid line).

Figure 12, panels a and b, are a plot of the elastic moduli of Figure 11 as a function of $\phi - \phi_{gel}$ and $\phi/\phi_{gel} - 1$, respectively. To convert the model calculations and experimental data of G' as a function of T of Figure 11 to G' as functions of $[\phi - \phi_{gel}]$ and $[\phi/\phi_{gel} - 1]$, one needs to know the gel boundary or how ϕ_{gel} changes as temperature is varied. For converting the experimental data, the power law curve fit of the experimental gel boundary (Figure 7) is used to get an expression for T_{gel} as a function of ϕ_{gel}. For the NMCT calculations in Figure 11, the gel boundary (Figure 2) at each value of κD is converted to T as a function of ϕ_{gel} by using the values of A and T_θ given in Table 3 for each κD. In Figure 12, panels a and b, the power law fits to the model calculations are given to reduce clutter and to make the graphs presentable. As can be seen from this figure, the scaling of $[\phi/\phi_{gel} - 1]$ collapses the experimental data and model calculations better than $[\phi - \phi_{gel}]$. Collapse of the experimental data with $[\phi/\phi_{gel} - 1]$ is in agreement with the data of Rueb and Zukoski,[28] who studied a similar system. The collapse of G'_{NMCT} with $[\phi/\phi_{gel} - 1]$ suggests this to be the correct scaling for the experimental system used in this work. The critical exponent p for the scaling as determined by curve fits of the experimental data is 1.7 ± 0.2 for the octadecyl silica/decalin system. In interpreting these graphs, it should still be kept in mind that NMCT does not rely on fractal or percolation models to predict G' and that the power law exponents arise from the temperature and volume fraction dependence of the localization length. In addition, NMCT does not inherently assume a volume fraction dependence that results in a particular volume fraction scaling.

To test the effectiveness of the model, a single value of A and T_θ with a constant κD of 11 is used to predict the measured elastic moduli. The values of A (27.8) and T_θ (307.5 K) used are

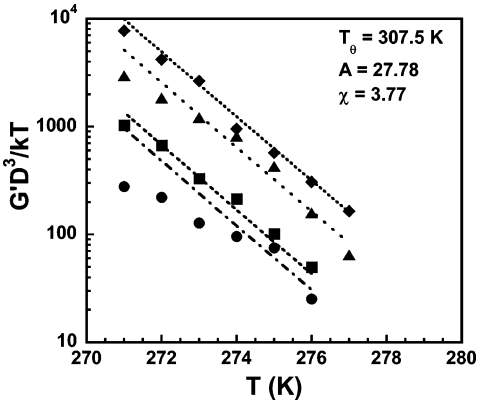

Figure 13. Scaled elastic modulus as a function of temperature at different volume fractions:: $\phi = 0.253$ (●), 0.306(■), 0.381(▲), and 0.446 (◆). The solid symbols are the experimental measurements of the elastic modulus. The dashed lines are calculations of the elastic modulus from eq 14 at a κD of 11 and at fixed values of A, T_θ, and χ. The average value of $(\kappa D)^2\phi/F^2$ which is required at $\kappa D = 11$ is calculated from eq 8 and is found to be 38.02.

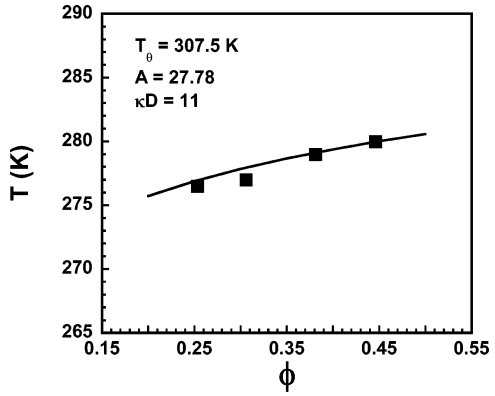

Figure 14. Gel boundary of the octadecyl silica system used in this work as a function of colloid volume fraction ϕ. The solid symbols are the experimental measurements while the line is the localization boundary calculated using NMCT with the Yukawa $S(q)$. A κD of 11 is used with $A = 27.78$ and $T_\theta = 307.5$ K, respectively.

the average of the values at ϕ of 0.306 and 0.381, respectively. The exponent χ at $\kappa D = 11$ is calculated from Table 2 and is averaged over all volume fractions at the particular κD. The averaging procedure yields a $\chi = 3.77$. The average value of $(\kappa D)^2\phi/F^2$ at $\kappa D = 11$ is calculated from eq 8 and is found to be 38.02. These values are then used in conjunction with eq 14 to predict the elastic moduli of the thermal gels. Comparisons of predictions with experimental data are shown in Figure 13. There is good agreement of experiments and model calculations at higher volume fractions ($\phi \geq 0.306$) and single values of A and T_θ do an excellent job of predicting the experimental measurements of elastic moduli. Figure 14 is a plot of the predicted gel boundary using the value of A and T_θ given above. As can be seen from Figure 14, constant values of A and T_θ are not only successful in predicting the elastic moduli but also in predicting the measured gel boundary.

The agreement of the NMCT calculations of the gel elastic modulus with experimental measurements of G' suggests several things. First, the absence of clustering in the experimental system is confirmed by the agreement of experiment and theory as NMCT does not take into account clustering in its formulation. This is independently seen in the scattering experiments which clearly show the absence of clusters. Clustering plays an important part in the case of depletion gels [21,22] where the particles are forced into clusters of 3−5 particle diameters and this fact has to be taken into account when predicting the strength of the resulting depletion gels. The cluster size in depletion gels is independent of volume fraction and polymer concentration, an experimental fact which is not yet well understood. It is these clusters which span space to give rise to a gel. Understanding the origin or the absence of clustering during gel formation, we feel, will lead to new insights about the mechanisms of gelation and the strength of the resulting materials. Second, the success of NMCT which uses the concept of localization length ($<D$) to predict G' suggests that the volume fraction dependencies of gel mechanical properties are dominated by density fluctuations of wave vector on the order of $2\pi/r_{loc}$ as opposed to $2\pi/D$ or smaller.

VI. Summary and Conclusions

In this study, we have extended the application of NMCT to predict the gel elastic modulus from depletion systems to a more general system in which colloidal particles interact with an attractive Yukawa potential (an effective one component interaction potential). Equations are developed for the prediction of the elastic modulus (G') once the pair interaction potential parameters κ^{-1} and ϵ and the suspension volume fraction are known. The model calculations are then compared with the experimental measurements of G' for a thermal gel system in which gelation is induced by reducing temperature. The key step in this comparison is to determine how the interaction potential parameters (κ^{-1} and ϵ) change with experimental variables. For the thermal gel system, we assume the strength of interaction ϵ/kT to have the form $A(T_\theta/T - 1)$ where A and T_θ are particle size and solvent dependent constants and T is the absolute temperature of the suspension. Once the parameters A and T_θ are fixed by matching the gel boundary and elastic modulus at one volume fraction, we find that we can predict almost quantitatively G' for all other ϕ and T. The success of NMCT coupled with the Yukawa potential in predicting the elastic moduli of thermal gels confirms the fact that one does not need to use fractal-based theories to predict the viscolelastic properties. The microstructure of the thermal gel system is in fact nonfractal at volume fractions greater than 0.2 as measured by scattering techniques. The success of the theory also suggests that the microscopic factor determining the elastic modulus is the localization length and if one predicts how the localization length varies inside the gel boundary then one can predict G'.

An important factor which needs to be taken into account before applying NMCT to different systems is that of clustering of particles. Depletion gels are composed of dense clusters and voids while this is absent in thermal gels. The presence of clusters in depletion gels reduces the strength of the elastic modulus and this has to be taken into account in the theoretical predictions of G' using NMCT. The presence and absence of clusters also highlights the nature of the interaction potential in the different systems.

The correlation developed in this work for the prediction of G' (eq 12) can be applied to a variety of systems in which particles experience attractions and hence gel. The key step is in relating the interaction potential parameters ϵ and κ^{-1} to experimentally measurable parameters. Applications of eq 12 to different systems (aggregated polystyrene lattices,[6] aggregated alumina[40]) will be reported in future publications.

Acknowledgment. We thank J. Bergenholtz for letting us use his code for calculating the structure factor of Yukawa potentials. We thank V. Gopalakrishnan and K. S. Schweizer for

(40) Channell, G. M.; Zukoski, C. F. *AIChE J.* **1997**, *43*, 1700.

their insights and discussions. We thank P.R. Jemian (UNICAT) for his assistance in gathering the scattering data. The UNICAT facility at the Advanced Photon Source (APS) is supported by the U.S. DOE under Award No. DEFG02-91ER45439, through the Frederick Seitz Materials Research Laboratory at the University of Illinois at Urbana-Champaign, the Oak Ridge National Laboratory (U.S. DOE Contract DE-AC05-00OR22725 with UT-Battelle LLC), the National Institute of Standards and Technology (U.S. Department of Commerce) and UOP LLC. The APS is supported by the U.S. DOE, Basic Energy Sciences, Office of Science under Contract No. W-31-109-ENG-38. Finally, we acknowledge financial support from the Nanoscale Science and Engineering Initiative of the National Science Foundation under NSF Award Number DMR-0117792.

LA060168J